Improvement of Slagging Monitoring and Soot-blowing of Waterwall in a 650MWe Coal-fired Utility Boiler

Ligang Xu[1, 2], Yaji Huang*[1], Junfeng Yue[3], Lu Dong[1], Lingqin Liu[1], Jianrui Zha[1], Mengzhu Yu[1], Bo Chen[3], Zhicheng Zhu[1], Hao Liu*[2]

1. Key Laboratory of Energy Thermal Conversion and Control of Ministry of Education, School of Energy and Environment, Southeast University, Nanjing, 210096, China

2. Faculty of Engineering, University of Nottingham, University Park, Nottingham, NG7 2RD, United Kingdom

3. Jiangsu Frontier Electric Technology Co., Ltd., Nanjing, 211102, China

Abstract: Owing to the lack of direct measurement on the slagging extent of the waterwall, random or empirical soot-blowing strategies practiced in many power plants can result in untimely or excessive soot-blowing operations. In this research, a dynamic slagging monitoring model was established based on the heat balance principle and GA-BP (genetic algorithm and backpropagation) neural networks. A soot-blowing optimization strategy was formulated by adopting the model of the maximum net heat profit and setting the accumulated system heat loss as the assessment variable. The applicability of the proposed monitoring model and optimization strategy was evaluated for the waterwall in a 650MWe coal-fired utility boiler. The monitoring results have verified that the change of system heat loss is in line with the actual slagging trend and the influence of the electric load change on the monitoring results is weakened greatly. The optimization results have shown that activating all soot blowers of the waterwall in every soot-blowing operation can achieve the higher net heat profit per unit time and the shorter duration for each pair of soot blowers. Using the optimized soot-blowing strategy can also realize the dynamic adjustment of the moment and the duration of soot-blowing, and improve the heat transfer performance of the waterwall remarkably.

Keywords: waterwall, slagging monitoring, GA-BP neural network, soot-blowing optimization, heat loss

1. Introduction

Owing to the important roles of coal-related industries in the energy sector and the global environment [1, 2], how to improve the power generation efficiency and reduce the coal consumption of coal-fired power plant boilers has become one of the most pursued technical challenges [3]. The ash-induced slagging and fouling problems are difficult to avoid for coal-fired boilers as coal always contains some mineral ash. Slagging and fouling can result in a serious deterioration of the heat transfer performance and the alkali metal salts in the deposited slag may cause corrosion problems [4, 5], especially when an off-design coal such as the Zhundong lignite with a high content of alkali elements is chosen for combustion [6, 7] by the boiler owner.

The slagging problem occurring at the furnace section is caused by the fused ash with complicated deposition mechanisms [8, 9] and is harder to be solved compared with the fouling. The most direct method for cleaning slag is the soot-blowing method. Almost all coal-fired utility boilers in China and the other parts of the world are equipped with effective soot blowers for eliminating the slagging of waterwall [10]. Nevertheless, due to the lack of direct measurement for the slagging degree in the furnace, the scheduled and quantitative soot-blowing strategies are empirically developed in most coal-fired power plants. An untimely soot-blowing can lead to a continuous decrease of the heat transfer performance of waterwall and an excessive soot-blowing can cause erosion problems in addition to wasting valuable steam.

To optimize the soot-blowing operation, the online slagging trend needs to be acquired prior to the operation [11, 12]. The direct methods for monitoring slagging mainly include monitoring the flue gas temperature and heat flux. Some researchers have recognized the flue gas temperature in the furnace as the key monitoring variable. Bilirgen et al. [13] analyzed the impact of the fuel composition, boiler operation parameters and soot-blowing behaviors on the slagging process by monitoring the furnace exit gas temperature to develop mitigation strategies. Zhang et al. [14, 15] monitored the flue gas temperature to reflect the slagging extent by the novel acoustic pyrometry technology. As there are so many factors that can affect the flue gas temperature of a utility boiler, the flue gas temperature can

only embody the change of slagging under certain stable conditions. Some scholars have considered installing the instruments on the waterwall for measuring the heat flux to show slagging tendency. For example, Teruel et al. [16] and Pena et al. [17] measured the heat flux under the actual and clean operation conditions by installing the heat flux meters, and then established the artificial neural networks based on the experimental data to predict the extent of slagging. Due to the violent combustion environment within the combustion furnace of a coal-fired power plant boiler, installing instruments on the waterwall and maintaining the instruments to work constantly are extremely difficult and can induce a significant additional cost to the plant owner, especially for the supercritical and ultra-supercritical boilers with lager design outputs. In addition to the direct monitoring methods, some researchers have developed the indirect monitoring model based on the energy balance to optimize the slag blowing operations. Taler et al. [18] developed a slag monitoring system based on the energy balance for the power plant boiler to provide a direct and quantitative assessment of the cleanliness in the furnace and convective surfaces. Romeo et al. [19, 20] built a monitoring system by combining the energy balance principle with the neural networks and fuzzy logic technologies to optimize boiler cleaning. These studies [18- 20] adopted the ratio between the real state parameters (absorbed heat or heat transfer coefficient) and the theoretically clean state parameters as the monitoring variable. The theoretically clean state parameters in the above studies were set by the design or empirical values, neglecting the influence of the off-design and varying operation conditions. Moreover, it is worth noting that some of the above studies [11, 17, 18] basically set a critical indicator based on the optimization model, and then compared the actual monitoring value with the pre-set critical value to judge the optimal soot-blowing moment. Assessing the instantaneous value of the monitoring variable completely relied on the accuracy of the monitoring results. Since the fluctuation of the monitoring results was unavoidable under the varying working conditions, the obtained optimal soot-blowing moment could well be unreliable.

The above literature review clearly shows that further investigations on slagging monitoring and soot-blowing optimization of utility boilers are still needed, especially considering their practical applications in utility boilers

are far from widespread or efficient. The aim of this work was to improve the slagging monitoring and soot-blowing of the waterwall in a 650MW coal-fired utility boiler. To achieve this aim, a dynamic slagging monitoring model was built by the heat balance principle and GA-BP (genetic algorithm and backpropagation) neural networks. Then, the soot-blowing optimization strategy was formulated based on the model of the maximum net heat profit and setting the accumulated system heat loss as the assessment variable. Finally, the applicability of the proposed monitoring model and optimization strategy was verified with the case study boiler where the monitored slagging trends were analyzed and the efficiency of the optimized soot-blowing was evaluated. The main novelty of this research includes defining the system heat loss as the monitoring variable, predicting the theoretically clean state parameters by GA-BP and setting the accumulated value of system heat loss, instead of the instantaneous value, as the assessment target, which ensures that the optimized soot-blowing strategy can realize both the dynamic adjustment and reliable judgment of the moment and the duration of soot-blowing. The established monitoring model and formulated optimization strategy do not require the use of additional instruments and hence can be widely applied in other similar utility boilers.

2. Methodology

2.1 Case study

A 650MWe supercritical utility boiler was used for the case study. The boiler maximum continuous rating (BMCR) is 2056t/h superheated steam at 571°C and 25.4MPa. Other main design parameters are listed in Table 1. As shown in Figure 1, the boiler is designed as a Π type layout with the single combustion chamber, balanced draft and solid slag discharge device. The main heat exchange surfaces include the waterwall, three stages of superheaters, two stages of reheaters, one economizer and two rotary air preheaters.

Table 1. Main design parameters of the boiler

Item	BMCR
Fuel (coal) mass flow	296 t/h
Main steam mass flow	2056 t/h
Superheated steam temperature	571 °C
Superheated steam pressure	25.4 MPa
Reheated steam flow	1716 t/h
Reheated steam temperature	569 °C
Reheated steam pressure	4.552 MPa
Feed water temperature	285 °C

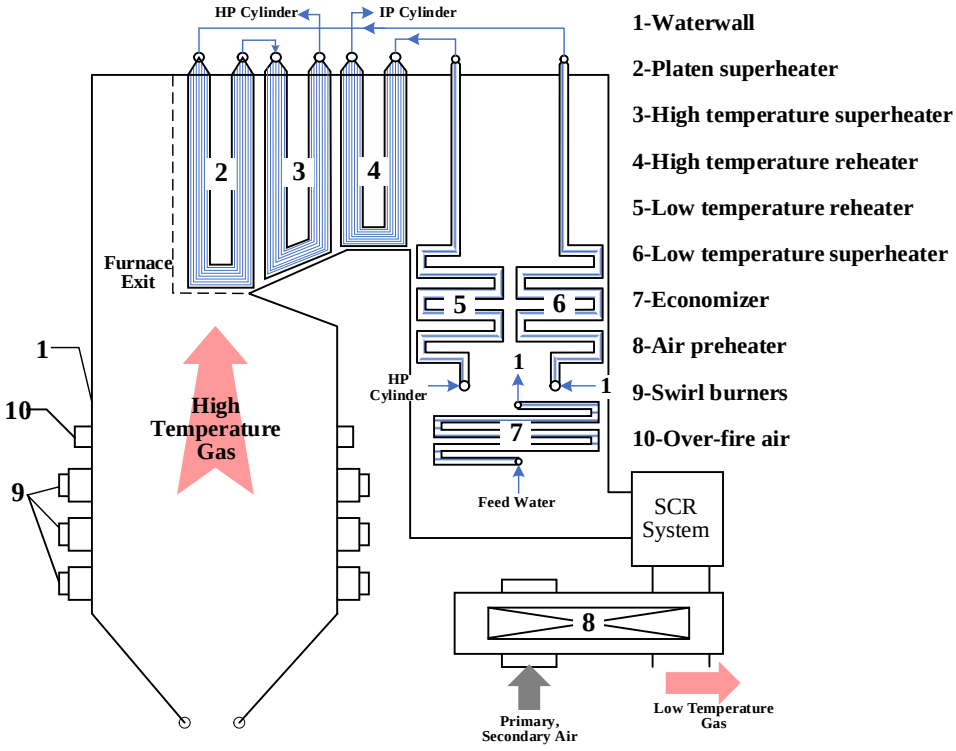

Figure 1. Schematic diagram of the utility boiler

The arrangement of burners and soot blowers are illustrated in Figure 2. The wall-fired combustion system contains three rows of swirl burners and one row of over-fire air nozzles. There are 98 soot blowers of waterwall arranged in six rows. From the bottom upwards, the A~C rows of soot blowers are only arranged on the two side walls (excluding the front wall and rear wall), and the D~F rows of soot blowers are arranged on four walls above the burners. Due to the consideration of saving steam energy, the current soot-blowing strategy in the power plant is that the D~F rows of soot blowers are activated twice or three times a day while the A~C rows of soot blowers are activated about once every three days. In every soot-blowing operation for the waterwall, all soot blowers are

activated sequentially and two soot blowers that symmetrically installed on the face-to-face walls are activated for 90s at the same time. Therefore, the normal operation duration of the D~F row blowers is approximately 54min (72÷2×90s) while the whole duration of all blowers (A~F) is approximately 73.5min (98÷2×90s). The steam for soot-blowing is extracted from the platen superheater outlet.

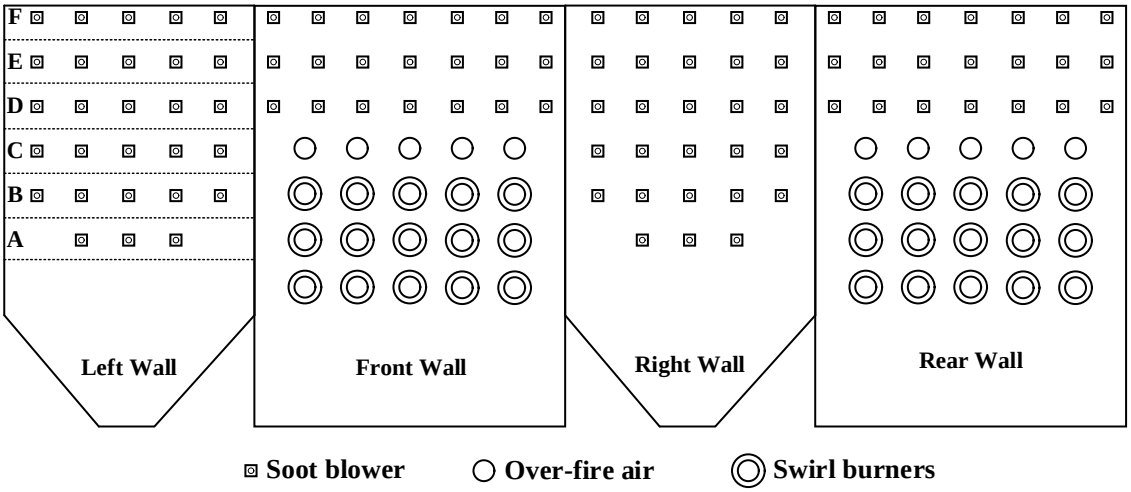

Figure 2. Arrangement of burners and soot blowers

In this work, the successive operating data of the utility boiler were collected for modeling and analysis, mainly including the parameters related to steam properties, flue gas and combustion performance. The samples of the coals burnt on different days were collected and used for the proximate and ultimate analysis. The moment and duration of the soot-blowing operation of waterwall were recorded. The collection interval of most data was 60s, while the collection interval of data within the first 600s after the soot-blowing operation of waterwall was 10s. The data preprocessing was conducted to reduce analysis errors. The outliers were detected when the mean value of the collected data is greater than three times its standard deviation and were replaced by the smoothed mean values [21, 22].

2.2 Slagging monitoring modeling

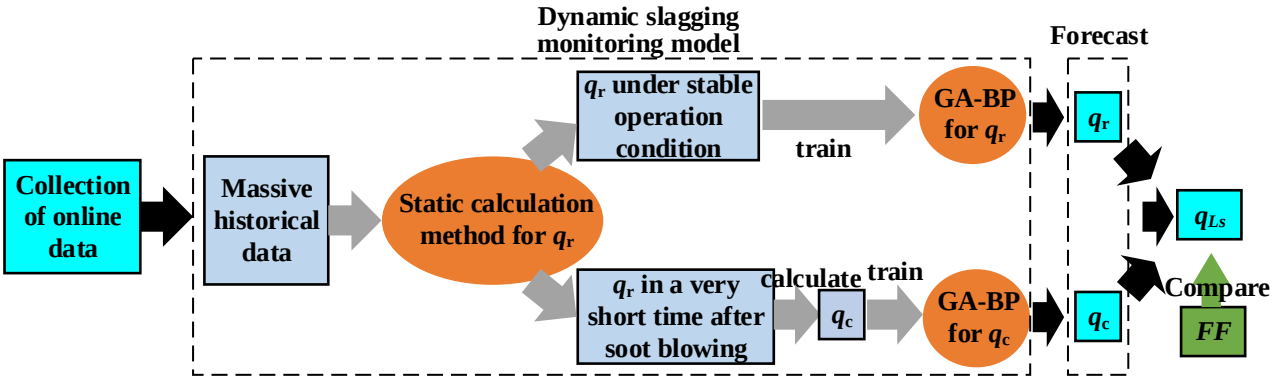

Figure 3. Flowchart of slagging monitoring

The whole flowchart of slagging monitoring is presented in Figure 3. The system heat loss q_{Ls} which is equal to the difference between the real and theoretically clean heat transfer capacities was used for monitoring (Eqn.(1)). It should be highlighted that the system heat loss in this research was specified as the heat loss of waterwall due to slagging. Besides, the conventional monitoring variable, the fouling factor *FF* (Eqn.(2)) based on the contrast between the real and theoretically clean heat transfer capacities was also calculated to compare the applicability. The real-time curves of q_{Ls} and *FF* were expected to be consistent with the changing trend of the slagging degree.

$$q_{Ls} = q_c - q_r \tag{1}$$

$$FF = 1 - \frac{q_r}{q_c} \tag{2}$$

where q_{Ls} is the system heat loss due to slagging (kW), q_r is the actual absorbed heat of waterwall (kW), q_c is the absorbed heat of the theoretically clean waterwall (kW).

In the slagging monitoring modeling, a static calculation method was first built to obtain q_r. Then, two GA-BP networks of q_r and q_c were established respectively. Base on the massive historical data, the calculated q_r under stable operating condition was used to train the GA-BP network of q_r, while the q_c based on the calculated q_r in a very short time after soot-blowing was used to train the GA-BP network of q_c. In the end, the trained GA-BP neural networks were utilized to forecast q_r and q_c online in the actual operation for the slagging monitoring.

2.2.1 Static calculation method for q_r

As the basic step for the monitoring model, a static calculation method based on the heat balance principle was

proposed by combining the heat transfer process of the furnace and semi-radiation heat exchange surfaces.

Firstly, the heat transfer model of furnace [23, 24] is given as Eqns. (3)~(4):

$$q_{\mathrm{r}} = \varphi B_{\mathrm{cal}} C_{\mathrm{av}} (T_{\mathrm{th}} - T_{\mathrm{f}}'') \tag{3}$$

$$q_{\mathrm{r}} = \psi \sigma_0 \varepsilon_{\mathrm{f}} T_{\mathrm{fl}}^4 H_{\mathrm{f}} \tag{4}$$

where ψ is average thermal effectiveness factor of the furnace, ε_{f} is furnace emissivity, σ_0 is Stefan–Boltzmann constant (5.67×10^{-11} kW/(m^2·K^4)), T_{fl} is hypothesis flame temperature (K), T_{th} is theoretical adiabatic combustion temperature (K, corresponding to the effective heat in the furnace), T_{f}'' is the furnace exit gas temperature, (the platen superheater inlet, K), φ is heat retention coefficient, B_{cal} is the calculated coal consumption (kg/s), C_{av} is the average specific heat capacity of gas in the furnace (kJ·kg^{-1}·K^{-1}), H_{f} is the heat transfer area of the furnace (m^2).

According to empirical statistical formula Eqn. (5), T_{fl} which is hard to be calculated or measured can be removed to obtain Eqn. (6) [25, 26].

$$T_{\mathrm{fl}}^4 = \frac{M^{\frac{5}{3}} T_{\mathrm{f}}'' T_{\mathrm{th}}^3}{\left(\frac{T_{\mathrm{th}}}{T_{\mathrm{f}}''} - 1\right)^{\frac{2}{3}}} \tag{5}$$

$$T_{\mathrm{f}}'' = \frac{T_{\mathrm{th}}}{M\left(\frac{\varepsilon_{\mathrm{f}} \sigma_0 \psi H_{\mathrm{f}} T_{\mathrm{th}}^3}{\varphi B_{\mathrm{cal}} C_{\mathrm{av}}}\right)^{0.6} + 1} \tag{6}$$

where M is the parameter related to the flame center and can be calculated by Eqn. (7) [26]. For the supercritical boiler, it is necessary to consider the attenuation of flame radiation intensity in the emission process [27]. ε_{f} should be calculated by Eqn. (8) and Eqn. (9).

$$M = 0.59 - 0.5\left(\frac{\sum_{1}^{i} B_i h_{\mathrm{b}i}}{h_{\mathrm{fc}} \sum_{1}^{i} B_i} + \Delta x_{\mathrm{b}}\right) \tag{7}$$

$$\varepsilon_{\mathrm{fl}} = \frac{\varepsilon_0}{0.32 k_{\mathrm{a}} R_{\mathrm{f}} \varepsilon_0 + 1} \tag{8}$$

$$\varepsilon_{\mathrm{f}} = \frac{\varepsilon_{\mathrm{fl}}}{\varepsilon_{\mathrm{fl}} + (1 - \varepsilon_{\mathrm{fl}})\psi} \tag{9}$$

where B_i, $h_{\mathrm{b}i}$ are the coal consumption and height of the i-th row of burners (kg/s, m), h_{fc} is the calculated height of furnace (m), Δx_{b} is the correction constant, ε_0 is the original flame emissivity, $\varepsilon_{\mathrm{fl}}$ is the actual flame emissivity

considering the radiation attenuation in the emission process, k_a is the radiation attenuation coefficient of flame (m^{-1}), R_f is the radius of furnace cross-section (m, conversed by area of rectangular cross-section).

ψ changes significantly with the extent of slagging because ψ represents the ratio of effective radiation to total radiation. Hence this variable shouldn't be set by the design value. T_f'' is an extremely high temperature that can't be gained constantly by ordinary measurement instruments so that the test point of T_f'' were not installed in most power plants. Therefore, ψ and T_f'' are the key variables that can only be calculated indirectly by other measured parameters. According to the field survey, the test point of gas temperature closest to the furnace exit is arranged at the high-temperature superheater outlet. So T_f'' can also be calculated by the heat balance of platen and high-temperature superheaters.

Secondly, the heat transfer equations of the platen and high-temperature superheaters can be combined and expressed as Eqns. (10)~(11) [24, 26, 28]:

$$D_1(h_1''-h_1')+D_2(h_2''-h_2')+q_{add}-k_{sp}q_f''=B_{cal}\varphi(I_f''-I_2''+\Delta\alpha I_k) \tag{10}$$

$$q_f''=\psi_{p,f}\varepsilon_f\sigma_0(T_f'')^4A_f \tag{11}$$

where D_1 and D_2 are the steam flow rates of platen and high-temperature superheater respectively (kg/s), h_1' and h_2' are the specific enthalpies of steam at the platen and high-temperature superheater inlet respectively (kJ/kg), h_1'' and h_2'' are the specific enthalpies of steam at the platen and high-temperature superheater outlet respectively (kJ/kg), I_f'' is the enthalpy of flue gas per unit coal consumption at the furnace exit (kJ/kg), I_2'' is the enthalpy of flue gas per unit coal consumption at the high-temperature superheater outlet (kJ/kg), q_{add} is the heat transfer quantity of the additional heating surface (kW), $\Delta\alpha$ is the total air leakage coefficient of the platen and high-temperature superheater, I_k is the enthalpy of air leakage per unit coal consumption (kJ/kg), k_{sp} is the ratio of radiation that platen and high-temperature superheater absorbed from the furnace exit, q_f'' is the direct radiation from the furnace exit (kW), A_f is the cross-sectional area of furnace exit (m^2), $\psi_{p,f}$ is the thermal effectiveness factor of the furnace exit. Note that there is a linear relationship between $\psi_{p,f}$ and ψ. k_{sp} is determined by the structures of heating surfaces and set by

the design value.

Finally, through combining the heat transfer models of the furnace, platen and high-temperature superheater, the proposed static calculation method for q_r is given as the following steps:

Step 1. Collecting real-time operational data.

Step 2. Assuming T_f'' and then calculating ψ by Eqn. (6).

Step 3. Calculating q_f'' by Eqn. (11) then calculate $(T_f'')_2$ by Eqn. (10).

Step 4. To output T_f'' and ψ when $|T_f''-(T_f'')_2|<1$, otherwise repeat Step 2~4.

Step 5. Calculating q_r by Eqn. (3) or Eqns. (4)~(5).

2.2.2 Dynamic monitoring model based on GA-BP

The calculation process of the static calculation method for q_r based on the heat balance was complicated and depended on the relatively stable working condition. The applicability of the static method was limited in actual operation especially the variable electric load. Besides, q_c representing the absorbed heat of the theoretically clean waterwall can't be calculated or measured directly. Therefore, in this study, the GA-BP neural network method was used to forecast q_r and q_c by training massive historical operating data.

The BP neural network is the widely used artificial neural network and is regarded as a gradient descent algorithm for supervised learning. But the BP neural network is very likely to converge to the local extremum when solving the global extremum of the complex nonlinear problem [29]. GA is an optimization method including characteristics of the population-based evolution, the survival of the fittest, directed stochastic, no dependence on the gradient information. The BP neural network optimized by GA is proved to perform well to obtain the global optimum extremum and minimize the forecast error [30, 31].

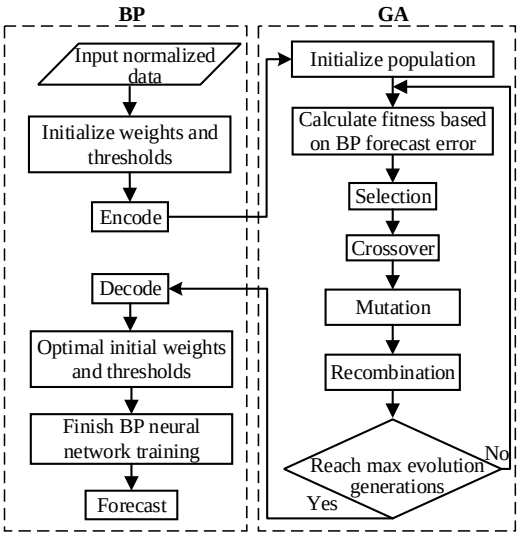

Figure 4. Flowchart of GA-BP neural network method

The flowchart of the GA-BP neural network method is illustrated in Figure 4. It can be seen that GA was adopted to optimize the initial weights and thresholds of the BP neural network to avoid local extremum. In the GA-BP method, the fitness is the mean absolute error (MAE) of BP forecast which can be calculated by Eqn. (12)

$$\mathrm{MAE} = \frac{1}{m}\sum_{k=1}^{m}\left|t_k - o_k\right| \tag{12}$$

where m is the number of test samples, t_k is the target value of k-th test sample, o_k is the predicted value of k-th test sample.

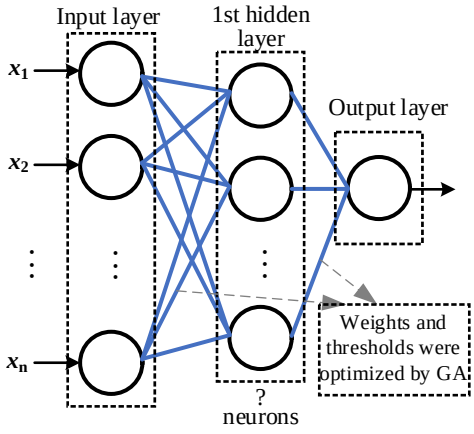

Figure 5. Structure of neural networks

The neural networks of q_r and q_c adopted a similar structure as shown in Figure 5. The tan-sigmoid function was used as the activation function. The number of hidden layers was set one which was actually enough for most engineering problems [29, 32]. The number of neurons in the hidden layer was set according to Eqn. (13) [30, 33].

Note that Eqn. (13) can only give the approximate range of n_h. Therefore, several GA-BP networks with different hidden neurons were trained to determine the optimum n_h by comparing the MAE. The mean absolute percentage error (MAPE) as given in Eqn. (14) was also calculated to evaluate the perdition accuracy.

$$n_h = \sqrt{n_{in} + n_{out}} + y \tag{13}$$

$$\mathrm{MAPE} = \frac{1}{m}\sum_{k=1}^{m}\left|\frac{t_k - o_k}{t_k}\right| \times 100\% \tag{14}$$

where n_{in}, n_{out} and n_h are the number of neurons in the input layer, output layer and hidden layer, respectively. y is a constant (within the range of 1~10).

The input parameters of the two networks are displayed in Table 2. There were 17 input parameters for the GA-BP network of q_r and 12 input parameters for the GA-BP network of q_c. For the two networks, the coal quality, combustion state and working condition were the three aspects for selecting the input parameters. All chosen parameters were able to be collected online or easily obtained, and this was why only the proximate analysis data of coal were selected to represent the coal quality. The coal consumption of the three rows of burners, the oxygen content of the flue gas, the temperature of the primary air and the temperature of the secondary air were selected to represent the combustion state. The flow rate of the feed water was selected to represent the electricity load of the working condition. The main difference between the two networks was whether the input parameters should reflect the influence of slagging or not. For the GA-BP network of q_r, the effect of slagging should be considered to acquire the actual heat transfer quantity. The furnace exit gas temperature T_f'' was supposed to be the optimal parameter to reflect the slagging process [13]. But T_f'' also needed to be calculated, so the parameters (13~17) in Table 2 were selected according to Eqn. (10). For the GA-BP network of q_c, the parameters with the impact of slagging should be removed to ensure the predicted output can reflect the absorbed heat of theoretically clean waterwall.

Table 2. Input parameters of the two networks

	Coal quality	Combustion state	Working condition
GA-BP network of q_r	1.moisture, 2.ash content, 3.sulfur content, 4.volatile, 5.net heating value	6. coal consumption of the 1st row of burners, 7. coal consumption of the 2nd row of burners, 8. coal consumption of the 3rd row of burners, 9. oxygen content of the gas flue, 10. temperature of the primary air, 11.temperature of the secondary air	12. flow rate of the feed water 13. steam temperature at the platen superheater inlet 14. steam pressure at the platen superheater inlet 15. steam temperature at the high-temperature superheater outlet 16. steam pressure at the high-temperature superheater outlet 17. gas temperature at the high-temperature superheater outlet
GA-BP network of q_c	1.moisture, 2.ash content, 3.sulfur content, 4.volatile, 5.net heating value	6. coal consumption of the 1st row of burners, 7. coal consumption of the 2nd row of burners, 8. coal consumption of the 3rd row of burners, 9. oxygen content of the gas flue, 10. temperature of the primary air, 11.temperature of the secondary air	12. flow rate of the feed water

In the learning stage of neural networks, the collected operating data of the utility boiler were calculated as learning data sets by the proposed static calculation method. For the q_r neural network training, the calculated actual q_r under stable operation conditions was used as the output parameter. For the q_c neural network training, the data collected within 600s after the soot-blowing operation of waterwall were adopted to calculate actual q_r. Then q_c was equal to the calculated actual q_r plus a constant as given in Eqn. (15).

$$q_c = q_r^{(600s)} + q_{c0} \tag{15}$$

where q_{c0} (kW) is a constant to ensure $q_c > q_r$ which can adopt the difference between the maximum value of q_r after soot-blowing and the BMCR design q_r.

All sets of data were normalized in the range of -1~1 to unify the evaluation criteria. And then the data sets were divided into 70% training subsets and 30% testing subsets. Half of the testing subsets were used for validation in the training process to avoid the over-fitting problem of networks. For the q_r neural network, 26927 sets of data were obtained under stable operating conditions. 18849 sets were selected as the training subsets while 8078 sets were selected as the testing subsets. For the q_c neural network, 2880 sets of data within 600s after the soot-blowing

operation of waterwall were obtained. 2016 sets were selected as the training subsets while 864 sets were selected as the testing subsets. Finally, through comparing the forecast errors (MAPE of the testing subsets) of GA-BP networks with different hidden neurons, the optimum GA-BP networks of q_r and q_c were confirmed.

2.3 Soot-blowing optimization strategy

Setting the standard and then making the judgment were two key parts for formulating a soot-blowing optimization strategy. In this research, the model of maximum net heat profit was adopted as the soot-blowing standard and the optimum soot-blowing moment was determined through assessing the accumulated system heat loss.

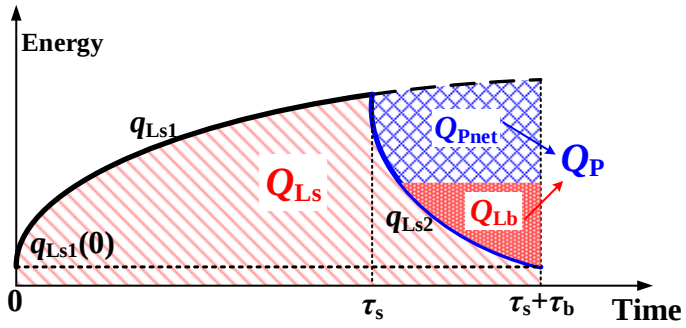

Figure 6. Change of heat loss and profit in a soot-blowing cycle

The operation process of the furnace can be divided into many soot-blowing cycles. A single soot-blowing cycle contained a period of the slagging process (τ_s) and a duration of soot-blowing (τ_b). Figure 6 depicts the change of heat loss and profit in a soot-blowing cycle. The system heat loss during the slagging process (q_{Ls1}) would increase sharply in the initial stage due to the rapid ash deposition [34, 35] and gradually tended to be flat, while the system heat loss during the soot-blowing period (q_{Ls2}) would dramatically drop. Q_{Ls} is the accumulated system heat loss in the soot-blowing cycle. Besides, soot-blowing brought the steam heat loss Q_{Lb} which increased linearly with τ_b. It was worth noting that the Q_P part between the curve of the hypothetical q_{Ls1} (dotted line) and actual q_{Ls2} (blue line) during the soot-blowing time was the whole heat profit due to the soot-blowing. The net heat profit (Q_{Pnet}) is the difference between Q_P and Q_{Lb}.

The net heat profit (Q_{Pnet}) is actually the improvement of the overall heat transfer quantity of furnace [36, 37].

The model of maximum heat profit aimed to maximize Q_{Pnet} per unit time by adjusting τ_{s} and τ_{b}. Hence the model for the soot-blowing optimization was given as Eqns. (16) and (17).

$$\max\left(\frac{Q_{\mathrm{Pnet}}}{\tau_{\mathrm{s}}+\tau_{\mathrm{b}}}=\frac{\int_{\tau_{\mathrm{s}}}^{\tau_{\mathrm{s}}+\tau_{\mathrm{b}}}\left(q_{\mathrm{Ls1}}(\tau)-q_{\mathrm{Ls2}}(\tau)\right)d\tau-\tau_{\mathrm{b}}q_{\mathrm{Lb}}}{\tau_{\mathrm{s}}+\tau_{\mathrm{b}}}\right) \tag{16}$$

$$s.t.\begin{cases}\text{(a) } q_{\mathrm{Ls1}}(\tau_{\mathrm{s}})=q_{\mathrm{Ls2}}(\tau_{\mathrm{s}})\\ \text{(b) } q_{\mathrm{Ls1}}(0)=q_{\mathrm{Ls2}}(\tau_{\mathrm{s}}+\tau_{\mathrm{b}})\\ \text{(c) } ①2160\mathrm{s}\le\tau_{\mathrm{b}}\le4320\mathrm{s}\ /\ ②2940\mathrm{s}\le\tau_{\mathrm{b}}\le5880\mathrm{s}\\ \text{(d) } \tau_{\mathrm{s}}+\tau_{\mathrm{b}}\ge21600\mathrm{s}\end{cases} \tag{17}$$

where q_{Lb} is steam heat loss (kW).

Eqn. (16) is the target function of which q_{Ls1} and q_{Ls2} were obtained based on the fitting curves of the massive historical data. Eqn. (17) includes the restraint conditions. The (a) restraint condition is to connect two curves of q_{Ls1} and q_{Ls2}. For the (b) restraint condition, it is expected that each soot-blowing can at least reach the initial cleaning state. The (c) restraint is a range for the duration of soot-blowing. As explained in section 2.1, due to the large area of waterwall, all soot blowers are evenly arranged on the whole waterwall. Each pair of soot blowers can only be operated 60s~120s to reduce the influence of high-temperature flame on the service life of soot blowers. Thereby, there were two soot-blowing modes: ①τ_{b} was set from 2160s (72÷2×60s) to 4320s (72÷2×120s) for the normal duration (D~F, 72 soot blowers) and ②τ_{b} was set from 2940s (98÷2×60s) to 5880s (98÷2×120s) for the whole duration (A~F, 98 soot blowers). These two modes would both be calculated and compared to analyze the applicability. Also, the erosion due to the excessive soot-blowing operation needed to be considered [38]. In this work, according to the safety requests from the power plant, the maximum frequency of soot-blowing operations for waterwall was set no more than four times a day as given in the (d) restraint.

Through solving the model of the maximum heat profit, the optimum slagging time (τ_{sopt}) and duration of soot-blowing (τ_{bopt}) can be acquired. The conventional soot-blowing schemes included the scheduled method that using fixed τ_{sopt} and τ_{bopt} directly or setting the fixed optimal system heat loss q_{Lsopt} or optimal fouling factor FF_{opt} as the assessing criteria. However, the actual operation condition was changing all the time as illustrated in Figure 7. The

scheduled soot-blowing scheme would ignore the actual slagging process. Using the fixed q_{Lsopt} or FF_{opt} as the assessing criteria heavily relied on the accuracy of the instantaneous value of q_{Ls} or FF. If the instantaneous values fluctuated significantly under unstable working conditions, judging the optimal soot-blowing moment may become difficult and unreliable.

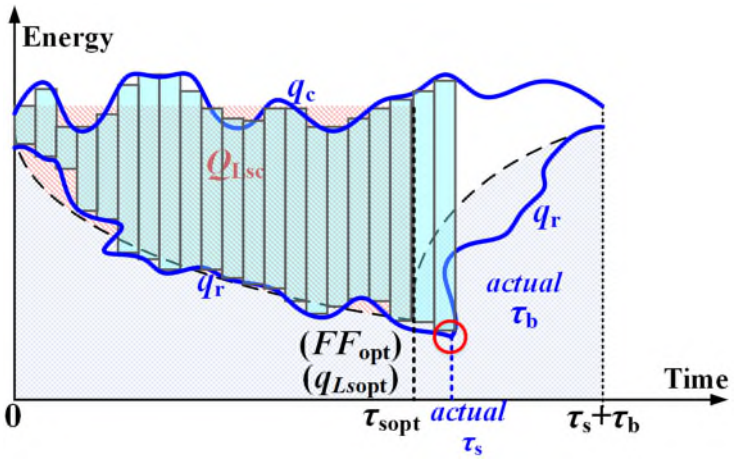

Figure 7. Change of heat transfer quantity in a soot-blowing cycle

Thus, the accumulated system heat loss Q_{Ls} was set as the assessment variable in this work and the critical system heat loss Q_{Lsc} was set as the assessing criteria. As given by Eqn. (18), Q_{Ls} would be calculated at each time of data collection and compared with Q_{Lsc} to judge the actual τ_{s}. Then the actual τ_{b} would also be adjusted according to the (b) restraint condition in Eqn. (17).

$$Q_{\mathrm{Ls}} \geq Q_{\mathrm{Lsc}} \Rightarrow \sum_{\mathrm{n=1}}^{\mathrm{now}} (q_{\mathrm{c}} - q_{\mathrm{r}}) \Delta\tau \geq \int_0^{\tau_{\mathrm{sopt}}} q_{\mathrm{Ls1}}(\tau) d\tau \tag{18}$$

where n is the number of data collection, $\Delta\tau$ is the collection interval.

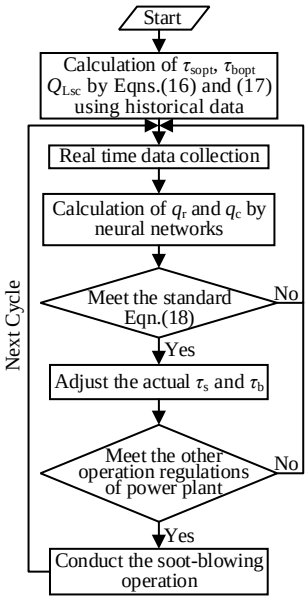

Figure 8. Flowchart of soot-blowing optimization strategy

The whole flowchart of the soot-blowing optimization strategy is depicted in Figure 8. It can be seen that the soot-blowing strategy can be adapted to the actual slagging situation because τ_s and τ_b would be re-adjusted.

3. Results and discussions

3.1 Validation of monitoring model

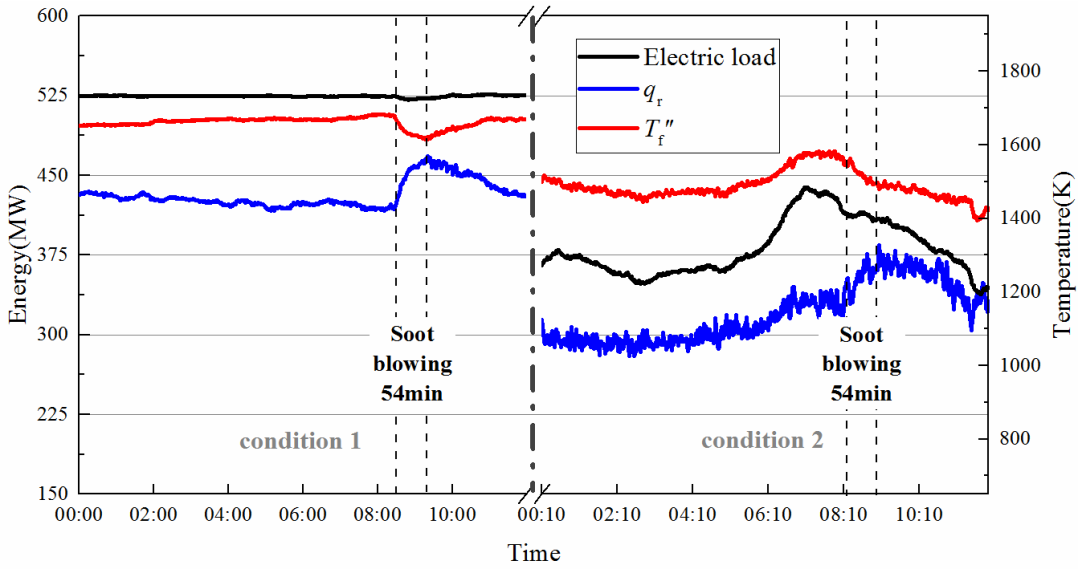

Figure 9. Change of electric load, q_r and T_f'' under stable load conditions (static method)

The trend of the calculated furnace exit gas temperature T_f'' which is the vital parameter of the furnace can be used to validate the static calculation method of q_r based on the heat balance principle [39]. Figure 9 displays the change of electric load, q_r and T_f'' under two stable load conditions. The load under condition 1 was approximately

constant, and hence the changes in the calculated q_r and T_f'' completely reflected the influence of slagging and soot-blowing. During the slagging period, the calculated q_r declined and T_f'' rose, representing the gradual deterioration of the heat transfer performance of waterwall. It was clear that q_r increased and T_f'' decreased during the soot-blowing period, representing the remarkable enhancement of the heat transfer performance of waterwall. The impact of the electric load on q_r and T_f'' was shown under condition 2 where the load was relatively stable but was also slowly changing. In fact, the general trends of q_r and T_f'' were consistent with the load [13, 40], which could also be observed under condition 2. It was noteworthy that q_r increased during the soot-blowing period which was opposite to the trend of the load, implying the apparent improvement of the heat transfer performance. In summary, the calculated q_r and T_f'' was basically in line with the actual situation, proving the static calculation method of q_r was applicable.

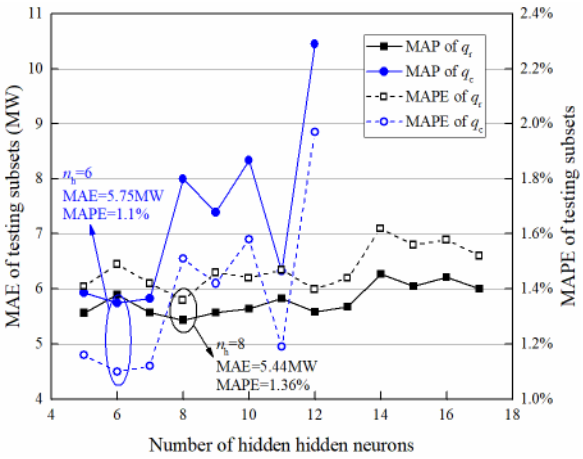

Figure 10. MAEs and MAPEs of GA-BP networks with different hidden neurons

The MAEs and MAPEs of several GA-BP networks with different hidden neurons are presented in Figure 10. As discussed in section 2.2.2, the hidden neurons were chosen according to Eqn. (13). It can be seen that the minimum MAE and MAPE of test subsets was achieved by the q_r network with 8 hidden neurons (5.44MW, 1.36%) and the q_c network with 6 hidden neurons (5.75MW, 1.10%), respectively. Therefore, the GA-BP network of q_r with 17 inputs, 8 hidden neurons and 1 output and the GA-BP network of q_c with 12 inputs, 6 hidden neurons and 1 output were utilized in this research.

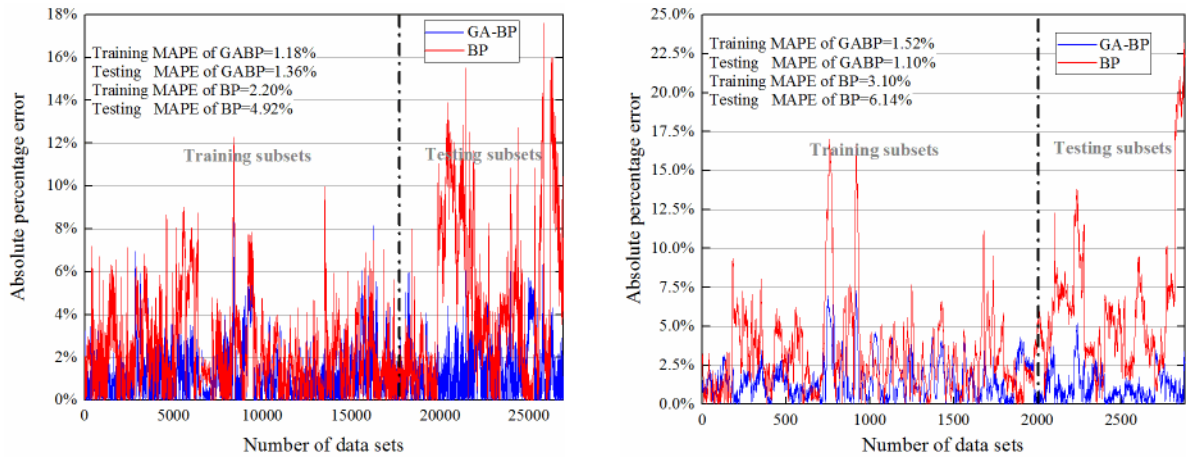

(a) Networks of q_r (b) Networks of q_c

Figure 11. Comparison of forecast errors between GA-BP and BP neural networks

The comparison of forecast errors between GA-BP and BP neural networks is shown in Figure 11. For the BP neural networks without any optimization, the absolute percentage error (APE) was quite large especially the APE of the testing subsets. The testing MAPEs of the BP networks of q_r and q_c were 4.92% and 6.14% respectively and much higher than the training MAPEs, reflecting the poor generalization performance of the BP neural networks. For the GA-BP neural networks with the genetic algorithm optimization, the APEs decreased significantly and were mainly lower than 2%. The testing MAPEs of GA-BP networks of q_r and q_c were basically close to the training MAPEs, showing the great generalization performance of GA-BP networks. Consequently, through analyzing the forecast performance from Figures 10~11, it was demonstrated that the established GA-BP networks of q_r and q_c were appropriate for the prediction.

3.2 Analysis of slagging monitoring results

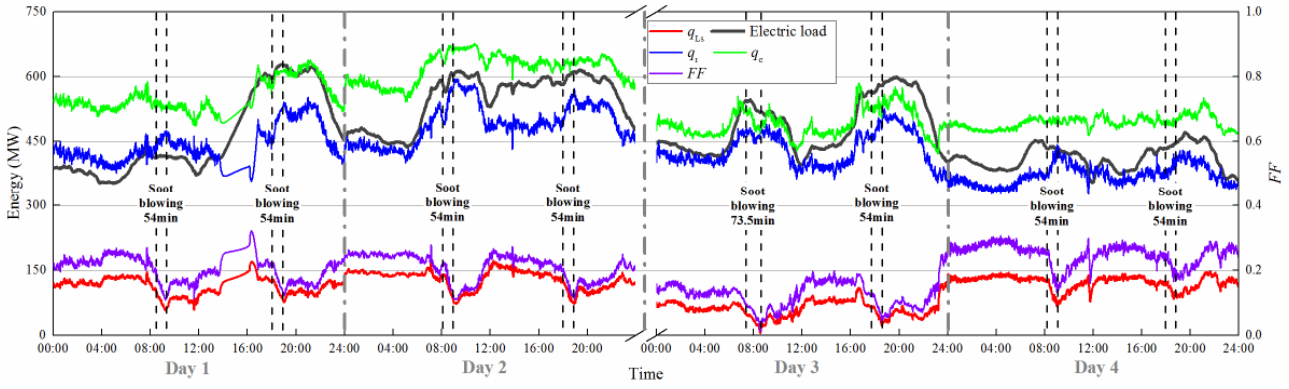

Figure 12. Slagging monitoring results of 4 days (including q_{Ls}, FF, electric load, q_r and q_c)

The slagging monitoring results including q_{Ls}, *FF*, electric load, q_r and q_c of 4 days are shown in Figure 12. It was clear that the case study boiler adopted a quantitative soot-blowing strategy. There were 8 soot-blowing operations in those 4 days, around twice a day. The normal soot-blowing duration was 54min while the 73.5min soot-blowing operation only occurred once, consistent with the description in section 2.1 that the A~C rows of soot blowers were activated about once every three days.

In general, the electric load had a strong correlation with q_r and q_c. Especially the change of q_c was consistent with the trend of the electric load, reflecting the theoretical clean heat transfer performance was determined by the plant load [16, 17]. The difference between the trends of q_r and q_c embodied the impact of slagging, which can be distinguished apparently during the soot-blowing period under three load trends. It can be seen from the soot-blowing period in Figure 12, when the load was unchanged, q_c stayed unchanged but q_r rose. When the load increased, q_r and q_c both increased but q_r rose more quickly. When the load decreased, q_c declined but q_r declined more slowly or even rose. The difference explained why q_{Ls} and *FF* based on the contrast between q_r and q_c can be selected as the monitor variable. The changes of q_{Ls} and *FF* were both in line with the actual slagging trend of waterwall and the influence of the electric load was largely eliminated. The q_{Ls} and *FF* ascended in the slagging process while q_{Ls} and *FF* descended remarkably during the soot-blowing period, directly reflecting the impact of the slagging on the heat transfer performance of waterwall.

It was noteworthy that even if the overall trend of monitoring results could meet the requirements, the small fluctuations of curves were inevitable. Furthermore, with the normal operation without the soot-blowing, sometimes it could be observed that q_{Ls} and *FF* decreased when the electric load rapidly rose. The decreases of q_{Ls} and *FF* were owing to the removal of ash deposition by the flue gas with a higher flow rate with the load increase [36, 41]. The flue gas with a higher flow rate brought more fused ash particles and blew away more deposited ash at the same time. When the flow rate flue gas increased too quickly, the removal effect was greater than the deposition effect, leading to the delay and even reducing the seriousness of the slagging process. If using *FF* as the monitoring variable,

the assessment method of the instantaneous value discussed in section 2.3 must be adopted. As shown in Figure 12, when the curve fluctuated or *FF* decreased due to the rapid growth of the electric load, it was hard and unreliable to judge the optimal soot-blowing moment according to the pre-set FF_{sopt}. So q_{Ls} was more appropriate than *FF* for formulating a flexible soot-blowing optimization strategy by assessing the accumulated system heat loss in Eqn. (18).

3.3 Evaluation of soot-blowing optimization

In order to solve the proposed soot-blowing optimization model in Eqns. (16) and (17), the fitting curve functions of the system heat loss during the slagging process (q_{Ls1}) and the system heat loss during the soot-blowing period (q_{Ls2}) must be acquired in advance. As shown in Figure 12, the initial value of q_{Ls} in different soot-blowing cycles was varied. Hence the specific starting value of fitting curves would be determined by the actual situation. The attention needed to be paid was the changing trend of fitting curves. In this work, the average trends of q_{Ls1} and q_{Ls2} were obtained based on historical data by the incremental statistic method.

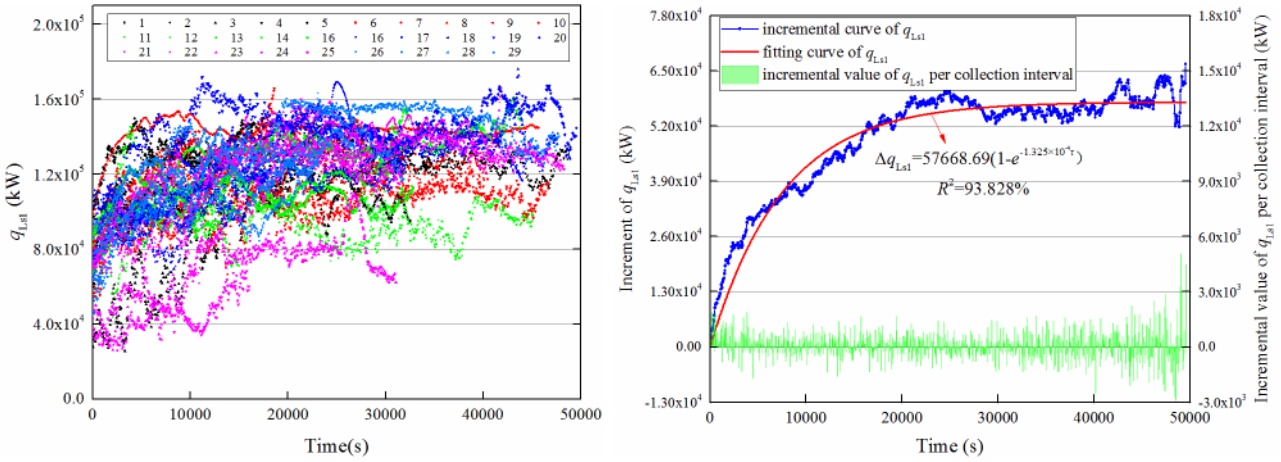

(a) Actual q_{Ls1} (b) Increment of q_{Ls1}

Figure 13. Actual, incremental and fitting curves of q_{Ls1}

The actual, incremental and fitting curves of q_{Ls1} are presented in Figure 13. In Figure 13(a), 29 actual q_{Ls1} curves under different working conditions were chosen to analyze the changing trend of q_{Ls1}. It can be seen that all curves had different starting values and durations, so it was inappropriate to directly averaging the values at the same moment of different curves. The average increments of multiple curves at different collection intervals were

calculated as bar charts in Figure 13(b). Then all the increments were summed up to form the incremental curve of q_{Ls1}. It was clear that the incremental curve of q_{Ls1} was consistent with the estimated trend in section 2.3, with the initial trend of rapid ascending and the subsequent trend of gradual flattening. The corresponding fitting function of q_{Ls1} was given in Eqn. (19).

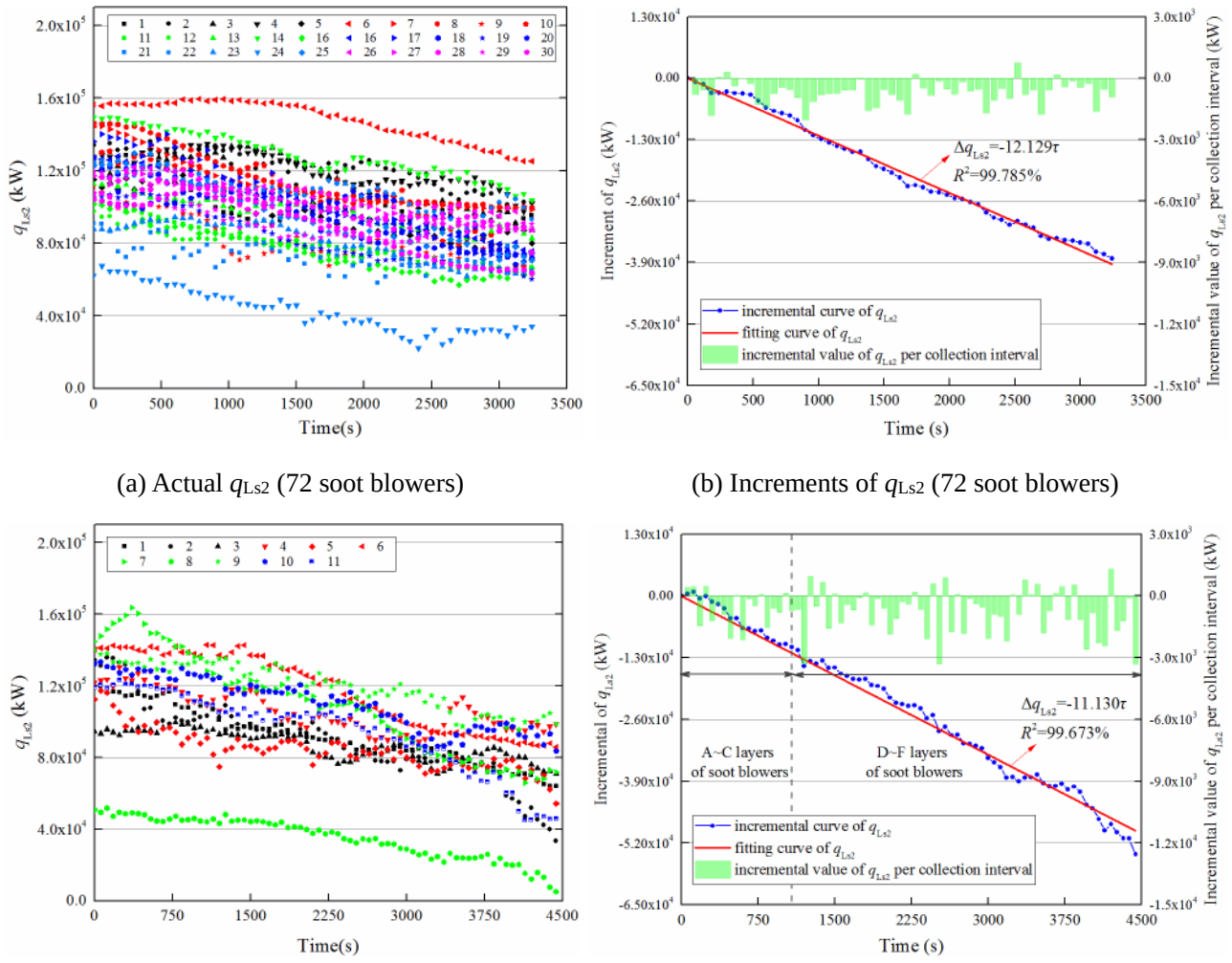

(a) Actual q_{Ls2} (72 soot blowers)

(b) Increments of q_{Ls2} (72 soot blowers)

(c) Actual q_{Ls2} (98 soot blowers)

(d) Increments of q_{Ls2} (98 soot blowers)

Figure 14. Actual, incremental and fitting curves of q_{Ls2}

The actual, incremental and fitting curves of q_{Ls2} are presented in Figure 14. For q_{Ls2}, there were two modes: ① the normal duration (D~F, 72 soot blowers) and ②the whole duration (A~F, 98 soot blowers). By the same incremental statistic method, the incremental curves of q_{Ls2} were obtained in Figure 14(b) and 14(d). It can be observed that the descending trend of curves was approximately linear. The corresponding linear fitting functions of Figure 14(b) and 14(d) are given in Eqn. (19). Note that the linear slopes of two soot-blowing modes were close,

showing that the efficiencies of two modes were similar.

$$\begin{cases} q_{Ls1}(\tau) = q_{Ls1}(0) + 57668.69(1 - e^{-1.325\times10^{-4}\tau}) & (\tau \geq 0, \text{s}) \\ \begin{cases} ①\, q_{Ls2}(\tau) = -12.129(\tau - \tau_s) + q_{Ls1}(\tau_s) \\ ②\, q_{Ls2}(\tau) = -11.130(\tau - \tau_s) + q_{Ls1}(\tau_s) \end{cases} & (\tau_s \leq \tau \leq \tau_s + \tau_b, \text{s}) \end{cases} \tag{19}$$

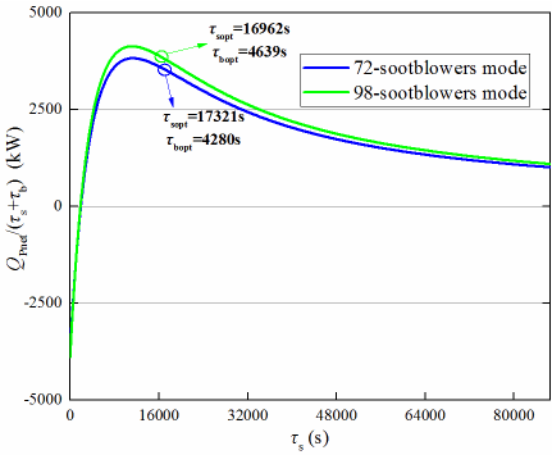

Figure 15. Changing trend of net heat profit per unit time ($Q_{Pnet}/(\tau_s+\tau_b)$) versus τ_s

According to the (b) constrain condition in Eqn. (17), τ_s and τ_b were linked, so solving Eqn. (16) was simplified into a single-variable optimization problem. The changing trend of the net heat profit per unit time ($Q_{Pnet}/(\tau_s+\tau_b)$) versus τ_s is displayed in Figure 15 and the calculated τ_{sopt} and τ_{bopt} are shown in Table 3. It can be seen that the maximum value of $Q_{Pnet}/(\tau_s+\tau_b)$ indeed existed. However, part of the heat profit had to be sacrificed according to the (d) restraint condition of Eqn. (17), because the frequency of soot-blowing should be limited to meet the safety requests for mitigating the erosion influence. It was worth noting that calculated τ_{bopt} of two soot-blowing modes were very close, while the duration for each pair of soot blowers is shorter and the $Q_{Pnet}/(\tau_s+\tau_b)$ was higher in the second mode. Thus, although it seemed that using 98 soot blowers would induce the increase of the steam loss, the higher $Q_{Pnet}/(\tau_s+\tau_b)$ could be achieved and the duration for each pair of soot blowers could be shortened to reduce the risk of erosion. So it was appropriate to activate all the soot blowers in every soot-blowing operation.

Table 3. The calculated τ_{sopt} and τ_{bopt} (one soot-blowing cycle)

Durations	①72 soot blowers	②98 soot blowers
τ_{sopt} (s)	17321	16962
τ_{bopt} (s)	4280	4639
the duration for each pair of soot blowers (s)	118.9	94.7

$Q_{Pnet}/(\tau_s+\tau_b)$ (kW)	3509.0	3808.5

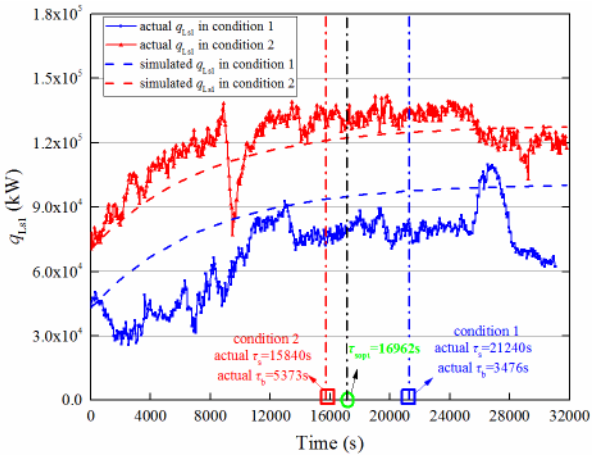

Figure 16. Optimization examples under two conditions (98 soot blowers mode)

As discussed in section 2.3, τ_{sopt} and τ_{bopt} were the recommended values, but the actual τ_s and τ_b would be adjusted by Eqn. (18) according to the actual slagging situation. Figure 16 exhibits the optimization examples under two conditions. The simulated curves were the calculated results of q_{Ls1} based on the fitting function in Eqn. (19). It can be seen that the actual τ_s would be ahead of τ_{sopt} when the growth rate of the actual q_{Ls1} exceeded the simulated growth rate, while the actual τ_s would be delayed when the growth rate of the actual q_{Ls1} was less than the simulated growth rate. Therefore, the timely adjustment of actual τ_s and τ_b can be realized and it was confirmed that using the accumulated value of the system heat loss for assessing was more flexible and reliable than the instantaneous value.

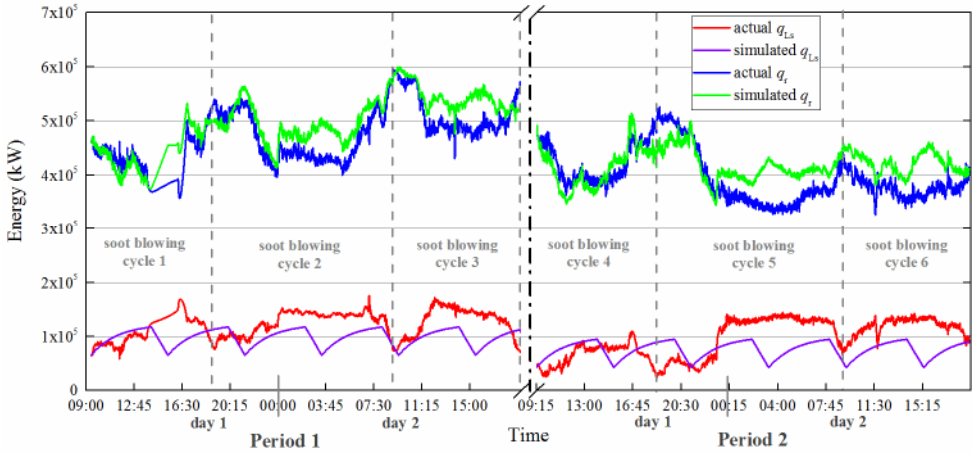

Figure 17. Comparison between actual values and simulated values of q_{Ls} and q_r

To evaluate the soot-blowing optimization, two periods including six complete soot-blowing cycles in Figure 12 were selected for analyzing. In evaluation, the scheduled soot-blowing strategy based on the fixed τ_{sopt} and τ_{bopt} (98

soot blowers) was adopted to estimate the improvement of heat transfer performance. The comparison between actual values and simulated values of q_{Ls} and q_r is displayed in Figure 17. The simulated q_{Ls} was calculated according to fitting functions with fixed τ_{sopt} and τ_{bopt}, so q_r can be acquired by original q_c. It can be seen that, at most time, the simulated q_r was obviously higher than the actual q_r after the simulated frequency of soot-blowing cycles were added.

Table 4. Optimization results (the scheduled soot-blowing strategy)

Parameters	Original	Optimization	Comparison
τ_s of each cycle (s)	Casual	16962	——
τ_b of each cycle (s)	3240	4639	+1399
Frequency of soot-blowing during period 1	3	5.6	+2.6
Frequency of soot-blowing during period 2	3	5.6	+2.6
net absorbed heat per unit time during period 1 (kW)	468640.72	492471.64	+5.09%
net absorbed heat per unit time during period 2 (kW)	395397.92	415763.14	+5.15%

The optimization results were shown in Table 4. The net absorbed heat (actual absorbed heat minus whole steam heat loss) per unit time of waterwall during two periods increased apparently by 5.09% and 5.15%, respectively. Thus, it can be concluded that the optimization of soot-blowing indeed improved the heat transfer performance of waterwall.

4. Conclusions

To solve the problem of empirical soot-blowing operations of the waterwall in a 650MWe coal-fired boiler, a dynamic slagging monitoring model was established based on the heat balance principle and the GA-BP neural networks and a soot-blowing optimization strategy was formulated by adopting the model of maximum net heat profit and setting the accumulated system heat loss as the assessment variable.

(1) The change of the system heat loss q_{Ls}, which was the monitoring variable used in this research, is consistent with the actual slagging trend of waterwall and the influence of electric load is largely reduced, validating the applicability of the monitoring model.

(2) The system heat loss q_{Ls} is more appropriate than the fouling factor *FF*, which is the conventional monitoring variable, for formulating a flexible soot-blowing optimization strategy by assessing the accumulated value of the system heat loss.

(3) The optimization results have shown that it is appropriate to activate all the soot blowers in every soot-blowing operation, achieving the higher net heat profit per unit time and the shorter duration for each pair of soot blowers.

(4) The optimized soot-blowing strategy can indeed enhance the heat transfer performance of the waterwall and can realize the dynamic adjustment and reliable judgment of actual τ_s and τ_b.

The established monitoring model and formulated optimization strategy do not require the use of additional instruments and hence can be widely applied in other similar utility boilers.

Acknowledgments

This work was supported by the National Key R&D Program of China (No. 2018YFB0605102), National Natural Science Foundation of China (No. 51676040) and Jiangsu Industrial Prospective and General Character Key Technology Project (No. BE2017037). The authors would also like to acknowledge the UK-China Joint Research and Innovation Partnership Fund PhD Placement Program and the scholarship from the China Scholarship Council (CSC), which enabled Ligang Xu to complete part of the reported work at the University of Nottingham.

Nomenclature

Abbreviation

APE	absolute percentage error
BMCR	boiler maximum continuous rating
BP	backpropagation neural network
FF	fouling factor
FF_{opt}	optimal fouling factor
GA	genetic algorithm
MAE	mean absolute error
MAPE	mean absolute percentage error

Symbol

A_f	cross-sectional area of furnace exit (m^2)
B_{cal}, B_i,	coal consumption of the boiler and the *i*-th row of burners, respectively (kg/s)
C_{av}	average specific heat capacity of gas in the furnace ($kJ \cdot kg^{-1} \cdot K^{-1}$)
D_1, D_2	steam flow rates of platen and high-temperature
Q_{Ls}	accumulated system heat loss (kW)
Q_{Lsc}	critical system heat loss (kW)
Q_P	whole heat profit due to the soot-blowing (kW)
Q_{Pnet}	net heat profit (kW)
q_{add}	heat transfer quantity of the additional heating surface (kW)
q_c	absorbed heat of the theoretically clean waterwall (kW)
q_{c0}	a constant to ensure $q_c > q_r$ (kW)
q_f''	direct radiation from the furnace exit (kW)
q_{Ls}	system heat loss (kW)
q_{Ls1}	system heat loss during the slagging process (kW)
q_{Ls2}	system heat loss during the soot-blowing period (kW)
q_{Lsopt}	optimal system heat loss (kW)
q_r	actual absorbed heat of waterwall (kW)
R_f	radius of furnace cross-section (m, conversed by area of

	superheater, respectively (kg/s)		rectangular cross-section)
H_f	heat transfer area of the furnace (m^2)	T_{fl}	hypothesis flame temperature (K)
h_{bi}	height of the *i*-th row of burners (m)	T_{th}	theoretical adiabatic combustion temperature (K)
h_{fc}	calculated height of furnace (m)	T_f''	furnace exit gas temperature (K)
h_1', h_2'	specific enthalpies of steam at the platen and high-temperature superheater inlet respectively (kJ/kg)	t_k	target value of *k*-th test sample
h_1'', h_2''	specific enthalpies of steam at the platen and high-temperature superheater outlet respectively (kJ/kg)	Δx_b	correction constant
I_2''	enthalpy of flue gas per unit coal consumption at the high-temperature superheater outlet (kJ/kg)	y	a constant (1~10)
I_f''	the enthalpy of flue gas per unit coal consumption at the furnace exit (kJ/kg)	$\Delta\alpha$	total air leakage coefficient of the platen and high-temperature superheater
I_k	enthalpy of air leakage per unit coal consumption (kJ/kg)	ε_f	furnace emissivity
k_a	radiation attenuation coefficient of flame (m^{-1})	ε_{fl}	actual flame emissivity
k_{sp}	ratio of radiation that platen and high-temperature superheater absorbed from the furnace exit	σ_0	Stefan–Boltzmann constant (5.67×10^{-11} kW/($m^2\cdot K^4$))
M	the parameter related to the flame center	τ_b	duration of soot-blowing (s)
m	number of test samples	τ_s	period of the slagging process (s)
n_{in}, n_{out}, n_h	number of neurons in the input layer, output layer and hidden layer, respectively	φ	heat retention coefficient
o_k	predicted value of *k*-th test sample	ψ	average thermal effectiveness factor of the furnace
Q_{Lb}	steam heat loss (kW)	$\psi_{p,f}$	thermal effectiveness factor of the furnace exit

References

[1]X. Liu, Y. Ge, G. Qi, S. Zhang, Review of simulation research on pulverized coal combustion in industrial boilers, IOP Conference Series: Earth and Environmental Science, 295(2019) 52028.

[2]L. Dong, H. Wang, Y. Huang, H. Chen, H. Cheng, L. Liu, L. Xu, J. Zha, M. Yu, S. Wang, Y. Duan, Elemental mercury removal from coal-fired flue gas using recyclable magnetic Mn-Fe based attapulgite sorbent, CHEMICAL ENGINEERING JOURNAL, (2020).

[3]P. Madejski, P. Żymełka, Calculation methods of steam boiler operation factors under varying operating conditions with the use of computational thermodynamic modeling, ENERGY, 197(2020) 117221.

[4]L. Xu, Y. Huang, J. Wang, C. Liu, L. Liu, L. Zou, J. Yue, K. Chen, Experimental investigation of high‐temperature corrosion properties in simulated reducing‐sulphidizing atmospheres of the waterwall fireside in the boiler, The Canadian Journal of Chemical Engineering, 98(2019) 905-918.

[5]S.C. Kung, Further Understanding of Furnace Wall Corrosion in Coal-Fired Boilers, CORROSION, 70(2014) 749-763.

[6]B. Wei, H. Tan, X. Wang, R. Ruan, Z. Hu, Y. Wang, Investigation on ash deposition characteristics during Zhundong coal combustion, JOURNAL OF THE ENERGY INSTITUTE, 91(2018) 33-42.

[7]X. Wang, Z. Xu, B. Wei, L. Zhang, H. Tan, T. Yang, H. Mikulčić, N. Duić, The ash deposition mechanism in boilers burning Zhundong coal with high contents of sodium and calcium: A study from ash evaporating to condensing, APPLIED THERMAL ENGINEERING, 80(2015) 150-159.

[8]L. Sun, H. Cai, Y. Zhang, S. Yang, Y. Qin, Research on the Fouling Prediction of Heat exchanger Based on Wavelet Neural Network, IEEE Conference on Cybernetics and Intelligent Systems, IEEE, 2008, pp. 999.

[9]Z. Ma, F. Iman, P. Lu, R. Sears, L. Kong, A.S. Rokanuzzaman, D.P. McCollor, S.A. Benson, A comprehensive slagging and fouling prediction tool for coal-fired boilers and its validation/application, FUEL PROCESSING TECHNOLOGY, 88(2007) 1035-1043.

[10]A. Pophali, B. Emami, M. Bussmann, H. Tran, Studies on sootblower jet dynamics and ash deposit removal in industrial boilers, FUEL PROCESSING TECHNOLOGY, 105(2013) 69-76.

[11]L. Pattanayak, S.P.K. Ayyagari, J.N. Sahu, Optimization of sootblowing frequency to improve boiler performance and reduce combustion pollution, Clean Technologies and Environmental Policy, 17(2015) 1897-1906.

[12]E. Diaz-Bejarano, F. Coletti, S. Macchietto, A Model-Based Method for Visualization, Monitoring, and Diagnosis of Fouling in Heat Exchangers, INDUSTRIAL & ENGINEERING CHEMISTRY RESEARCH, 59(2020) 4602-4619.
[13]H. Bilirgen, Slagging in PC boilers and developing mitigation strategies, FUEL, 115(2014) 618-624.
[14]S. Zhang, G. Shen, L. An, G. Li, Ash fouling monitoring based on acoustic pyrometry in boiler furnaces, APPLIED THERMAL ENGINEERING, 84(2015) 74-81.
[15]S. Zhang, G. Shen, L. An, Y. Niu, G. Jiang, Monitoring ash fouling in power station boiler furnaces using acoustic pyrometry, CHEMICAL ENGINEERING SCIENCE, 126(2015) 216-223.
[16]E. Teruel, C. Cortés, L. Ignacio Díez, I. Arauzo, Monitoring and prediction of fouling in coal-fired utility boilers using neural networks, CHEMICAL ENGINEERING SCIENCE, 60(2005) 5035-5048.
[17]B. Pena, E. Teruel, L.I. Diez, Soft-computing models for soot-blowing optimization in coal-fired utility boilers, APPLIED SOFT COMPUTING, 11(2011) 1657-1668.
[18]J. Taler, D. Taler, Slag Monitoring System for Combustion Chambers of Steam Boilers, HEAT TRANSFER ENGINEERING, 30(2009) 903-911.
[19]L.M. Romeo, R. Gareta, Hybrid System for fouling control in biomass boilers, ENGINEERING APPLICATIONS OF ARTIFICIAL INTELLIGENCE, 19(2006) 915-925.
[20]L.M. Romeo, R. Gareta, Neural network for evaluating boiler behaviour, APPLIED THERMAL ENGINEERING, 26(2006) 1530-1536.
[21]Y. Shi, Q. Li, J. Wen, F. Cui, X. Pang, J. Jia, J. Zeng, J. Wang, Soot Blowing Optimization for Frequency in Economizers to Improve Boiler Performance in Coal-Fired Power Plant, Energies, 12(2019) 2901.
[22]S.A. Kumari, S. Srinivasan, Ash fouling monitoring and soot-blow optimization for reheater in thermal power plant, APPLIED THERMAL ENGINEERING, 149(2019) 62-72.
[23]W. Bai, Y. Zhang, Y. Yang, H. Li, M. Yao, 300 MW boiler design study for coal-fired supercritical CO2 Brayton cycle, APPLIED THERMAL ENGINEERING, 135(2018) 66-73.
[24]J. Wu, H. Hou, E. Hu, Y. Yang, Performance improvement of coal-fired power generation system integrating solar to preheat feedwater and reheated steam, SOLAR ENERGY, 163(2018) 461-470.
[25]Y. Zhang, Q. Li, J. Feng, Theory and Calculation of Heat Transfer in Furnace, Tsinghua University Press, Beijing, 2008.
[26]D. Che, Boilers—Theroy, Design and Operation, Xi'an Jiaotong University Press, Xi'an, 2008.
[27]Q. Zhou, L. Zhao, Study on radiation heat transfer in boiler furnaces by taking radiant intensity attenuation in cross section into consideration, Journal of Southeast University, 38(2008) 1004-1010.
[28]S. Tong, X. Zhang, Z. Tong, Y. Wu, N. Tang, W. Zhong, Online Ash Fouling Prediction for Boiler Heating Surfaces based on Wavelet Analysis and Support Vector Regression, Energies, 13(2020) 59.
[29]S. Haykin, Neural Networks and Learning Machines, 3/E ed., Pearson Education India, 2010.
[30]S. Wang, J. Wang, F. Shang, Y. Wang, Q. Cheng, N. Liu, A GA-BP method of detecting carbamate pesticide mixture based on three-dimensional fluorescence spectroscopy, SPECTROCHIMICA ACTA PART A-MOLECULAR AND BIOMOLECULAR SPECTROSCOPY, 224(2020) 117396.
[31]S. Tang, M. Li, F. Wang, Y. He, W. Tao, Fouling potential prediction and multi-objective optimization of a flue gas heat exchanger using neural networks and genetic algorithms, INTERNATIONAL JOURNAL OF HEAT AND MASS TRANSFER, 152(2020) 119488.
[32]S. Karsoliya, Approximating number of hidden layer neurons in multiple hidden layer BPNN architecture, International Journal of Engineering Trends and Technology, 3(2012) 714-717.
[33]M. Madhiarasan, S.N. Deepa, A novel criterion to select hidden neuron numbers in improved back propagation networks for wind speed forecasting, APPLIED INTELLIGENCE, 44(2016) 878-893.
[34]X. Yang, D. Ingham, L. Ma, H. Zhou, M. Pourkashanian, Understanding the ash deposition formation in Zhundong lignite combustion through dynamic CFD modelling analysis, FUEL, 194(2017) 533-543.
[35]C. Luan, C. You, D. Zhang, An experimental investigation into the characteristics and deposition mechanism of high-

viscosity coal ash, FUEL, 119(2014) 14-20.
[36]Y. Shi, J. Wang, Z. Liu, On-line monitoring of ash fouling and soot-blowing optimization for convective heat exchanger in coal-fired power plant boiler, APPLIED THERMAL ENGINEERING, 78(2015) 39-50.
[37]Z. Yu-dong, Y. Wei-ping, O.U. Zong-xian, Application of Entropy Generation Analysis on Research of Sootblowing Optimization for Boiler, Proceedings of the Chinese Society of Electrical Engineering, 28(2008) 13-17.
[38]W. Wojnar, Erosion of heat exchangers due to sootblowing, ENGINEERING FAILURE ANALYSIS, 33(2013) 473-489.
[39]J.S. Chandok, I.N. Kar, S. Tuli, Estimation of furnace exit gas temperature (FEGT) using optimized radial basis and back-propagation neural networks, ENERGY CONVERSION AND MANAGEMENT, 49(2008) 1989-1998.
[40]A.K. Sivathanu, S. Subramanian, P. Ramalingam, Detection of Ash Fouling in Thermal Power Plant, NATIONAL ACADEMY SCIENCE LETTERS-INDIA, 41(2018) 369-373.
[41]Y. Cai, K. Tay, Z. Zheng, W. Yang, H. Wang, G. Zeng, Z. Li, S. Keng Boon, P. Subbaiah, Modeling of ash formation and deposition processes in coal and biomass fired boilers: A comprehensive review, APPLIED ENERGY, 230(2018) 1447-1544.